





## RESEARCH ARTICLE

# Hippocampal position and orientation as prognostic biomarkers for posttraumatic epileptogenesis: An experimental study in a rat lateral fluid percussion model

Riccardo De Feo<sup>1,2</sup>  | Eppu Manninen<sup>1</sup>  | Karthik Chary<sup>1</sup> | Elina Hämäläinen<sup>1</sup> | Riikka Immonen<sup>1</sup> | Pedro Andrade<sup>1</sup> | Xavier Ekolle Ndode-Ekane<sup>1</sup> | Olli Gröhn<sup>1</sup> | Asla Pitkänen<sup>1</sup>  | Jussi Tohka<sup>1</sup> 

<sup>1</sup>A. I. Virtanen Institute for Molecular Sciences, University of Eastern Finland, Kuopio, Finland

<sup>2</sup>Sapienza University of Rome, Rome, Italy

## Correspondence

Jussi Tohka, A. I. Virtanen Institute for Molecular Sciences, University of Eastern Finland, Neulaniementie 2, FI-70150 Kuopio, Finland.  
Email: [jussi.tohka@uef.fi](mailto:jussi.tohka@uef.fi)

## Funding information

National Institute of Neurological Disorders and Stroke, Grant/Award Number: U54NS100064; Sigrid Juselius foundation; European Social Fund, Grant/Award Number: S21770; Seventh Framework Programme, Grant/Award Number: 602102; Pohjois-Savon Rahasto, Grant/Award Number: 65211916; Academy of Finland, Grant/Award Number: 2285733-9, 272249, 273909, 298007 and 316258

## Abstract

**Objective:** This study was undertaken to identify prognostic biomarkers for post-traumatic epileptogenesis derived from parameters related to the hippocampal position and orientation.

**Methods:** Data were derived from two preclinical magnetic resonance imaging (MRI) follow-up studies: EPITARGET (156 rats) and Epilepsy Bioinformatics Study for Antiepileptogenic Therapy (EpiBioS4Rx; University of Eastern Finland cohort, 43 rats). Epileptogenesis was induced with lateral fluid percussion-induced traumatic brain injury (TBI) in adult male Sprague Dawley rats. In the EPITARGET cohort,  $T_2^*$ -weighted MRI was performed at 2, 7, and 21 days and in the EpiBioS4Rx cohort at 2, 9, and 30 days and 5 months post-TBI. Both hippocampi were segmented using convolutional neural networks. The extracted segmentation mask was used for a geometric construction, extracting 39 parameters that described the position and orientation of the left and right hippocampus. In each cohort, we assessed the parameters as prognostic biomarkers for posttraumatic epilepsy (PTE) both individually, using repeated measures analysis of variance, and in combination, using random forest classifiers.

**Results:** The extracted parameters were highly effective in discriminating between sham-operated and TBI rats in both the EPITARGET and EpiBioS4Rx cohorts at all timepoints ( $t$ ; balanced accuracy > .9). The most discriminating parameter was the inclination of the hippocampus ipsilateral to the lesion at  $t = 2$  days and the volumes at  $t \geq 7$  days after TBI. Furthermore, in the EpiBioS4Rx cohort, we could effectively discriminate epileptogenic from nonepileptogenic animals with a longer MRI follow-up, at  $t = 150$  days (area under the curve = .78, balanced accuracy = .80,  $p = .0050$ ), based on the orientation of both hippocampi. We found that the ipsilateral hippocampus rotated outward on the horizontal

Asla Pitkänen and Jussi Tohka are joint senior authors.

This is an open access article under the terms of the [Creative Commons Attribution-NonCommercial](https://creativecommons.org/licenses/by-nc/4.0/) License, which permits use, distribution and reproduction in any medium, provided the original work is properly cited and is not used for commercial purposes.

© 2022 The Authors. *Epilepsia* published by Wiley Periodicals LLC on behalf of International League Against Epilepsy

plane, whereas the contralateral hippocampus rotated away from the vertical direction.

**Significance:** We demonstrate that assessment of TBI-induced hippocampal deformation by clinically translatable MRI methodologies detects subjects with prior TBI as well as those at high risk of PTE, paving the way toward subject stratification for antiepileptogenesis studies.

#### KEYWORDS

hippocampal geometry, machine learning, MRI, posttraumatic epilepsy, random forest

## 1 | INTRODUCTION

Globally, an estimated 2.4 million people are diagnosed with epilepsy each year.<sup>1</sup> In 60% of those affected, epileptogenesis is initiated by structural causes such as traumatic brain injury (TBI).<sup>2</sup> Approximately 20 hypothesis-driven intervention approaches have demonstrated some disease-modifying effect in animal models of posttraumatic epilepsy (PTE), resulting in reduced seizure susceptibility and/or milder epilepsy.<sup>3</sup> However, no clinical treatments are available to stop or alleviate epileptogenesis in at-risk TBI patients or to alleviate the course of PTE after its diagnosis. One major reason for the stalled progression of interventions to clinical antiepileptogenesis trials is the lack of prognostic biomarkers that could be used to stratify patient populations for antiepileptogenesis trials and reduce study costs, making sufficiently powered clinical trials affordable.<sup>4</sup>

Epidemiological studies have shown that PTE develops in 16%–20% of patients with severe TBI.<sup>5,6</sup> Retrospective follow-up studies indicated that in approximately 80%, PTE was diagnosed within 2 years, and in 60%, within 1 year after TBI.<sup>5–7</sup> The seizure onset zone was in the temporal lobe in 57% and frontal lobe in 35% of patients.<sup>8</sup> Video-electroencephalographic (EEG) monitoring follow-ups in several laboratories have also demonstrated posttraumatic epileptogenesis in rodents with TBI.<sup>3</sup> The most often used animal model of PTE is induced with lateral fluid percussion injury (FPI), triggering epileptogenesis in approximately 25% of rats with severe TBI by 6 months postinjury.<sup>9–14</sup> As in humans, the seizure onset zone in rats with PTE develops in the lesioned cortex.<sup>12,15,16</sup> In addition to neocortical damage, TBI and PTE patients as well as rodents show hippocampal histopathology.<sup>17</sup> Furthermore, 44% of patients with temporal lobe seizure onset had mesial temporal sclerosis.<sup>8</sup> In animal models, slice electrophysiology studies in a lateral FPI model have demonstrated hippocampal hyperexcitability as well as histopathology comparable to hippocampal sclerosis.<sup>18,19</sup> Moreover, Kharatishvili et al.<sup>19</sup> found that the severity

### Key Points

- Using a geometric construction, 39 hippocampal parameters describing the orientation and relative positioning of the hippocampi were extracted
- Training random forest classifiers, we accurately discriminated between sham-operated and TBI rats from 2 days to 5 months postsurgery
- At 5 months postsurgery, epileptic and nonepileptic animals were distinguished based on hippocampal geometry with 80% accuracy
- We visualize the most discriminating changes between epileptic and nonepileptic rats

of hippocampal histopathology and magnetic resonance imaging (MRI) diffusivity were associated with hyperexcitability. Hayward et al.<sup>20</sup> reported that enhanced seizure susceptibility was associated with reduced cerebral blood flow in the ipsilateral hippocampus at 9 months post-TBI. Shultz et al.<sup>10</sup> indicated that changes in hippocampal surface morphometry at 6 months post-TBI differentiated rats with or without epilepsy after lateral FPI. Lastly, Pitkänen and Immonen<sup>21</sup> showed that increased diffusivity in the ipsilateral hippocampus at 9 days predicted increased seizure susceptibility at 12 months post-TBI. Taken together, these data suggest that hippocampal changes are part of the epileptogenic network after TBI. However, the number of studied animals, so far, has been relatively low, too limited to predict epileptogenesis after TBI with high accuracy.

The present study was designed to test the hypothesis that parameters indicating post-TBI structural changes in the hippocampus could present prognostic biomarkers for posttraumatic epileptogenesis. We utilized two large MRI datasets of rats with lateral FPI, one generated in the European Union-funded study EPITARGET and another in the National Institutes of Health-funded Centers

Without Walls project Epilepsy Bioinformatics Study for Antiepileptogenic Therapy (EpiBioS4Rx). We automatically segmented all samples using MU-Net-R,<sup>22</sup> a convolutional neural network (CNN),<sup>23</sup> which reduces bias for healthy anatomy compared to atlas registration-based segmentation methods. Using a geometric construction, we then extracted 39 anatomical parameters for each animal at each timepoint and analyzed their effectiveness in discriminating between (1) sham-operated experimental control and TBI rats and (2) TBI rats with (TBI+) and without (TBI-) epilepsy. We evaluated each parameter separately in a mass univariate analysis, and by combining them using random forest classifiers. Our data show that both approaches were highly effective in discriminating between sham and TBI rats. Moreover, the anatomical biomarkers described here can effectively discriminate between TBI+ and TBI- rats at 5 months after TBI. Although machine learning approaches for the detection of epilepsy have found several applications in both imaging and nonimaging diagnostics,<sup>24</sup> our novel approach provides interpretable results outlining some of the changes in hippocampal geometry as a result of epileptogenesis.

## 2 | MATERIALS AND METHODS

The number of animals in the two cohorts is summarized in Table 1. In the power calculation (power = .8,  $p < .05$ , MedCalc software), we expected a 25% epilepsy rate based on previous studies.<sup>3</sup> The biomarker was expected to have an area under the curve (AUC) > .850. Thus, we would need 7 TBI+ and 21 TBI- animals. We describe only the details that are important for the present study. A detailed description of the methods pertaining to the induction of TBI and video-EEG monitoring is presented in Appendix S1.

All experiments were approved by the animal ethics committee of the provincial government of Southern Finland and performed in accordance with the guidelines of the European Community Council Directives 2010/63/EU.

**TABLE 1** Number of magnetic resonance imaging scans per cohort (EpiBioS4Rx, EPITARGET) at different timepoints and in different treatment groups (TBI, sham-operated experimental controls)

Timepoints	Sham	TBI-	TBI+
EpiBioS4Rx			
2, 9, 30, 150 days	11	23	9
EPITARGET			
2, 21 days	23	84	29
7 days	23	82	29

Abbreviations: EpiBioS4Rx, Epilepsy Bioinformatics Study for Antiepileptogenic Therapy; TBI, traumatic brain injury.

## 2.1 | Animal cohorts

### 2.1.1 | EPITARGET cohort

EPITARGET (<https://epitarget.eu/>) was a European Union Framework 7-funded, large-scale, multidisciplinary research project aimed at identifying mechanisms and treatment targets for epileptogenesis after various epileptogenic brain insults. The EPITARGET cohort consisted of 23 sham-operated controls and 113 rats with TBI induced with lateral FPI (29 TBI+ and 84 TBI-). The 6-month MRI follow-up of the EPITARGET animal cohort has been described in detail previously.<sup>25</sup>

#### Animals

Adult male Sprague Dawley rats (Envigo Laboratories) were used. They were single-housed in a controlled environment (temperature = 21–23°C, humidity = 50%–60%, lights on 7:00 a.m. to 7:00 p.m.) with free access to food and water. Severe traumatic brain injury ( $3.26 \pm .08$  atm) was induced in the left hemisphere by lateral fluid percussion under pentobarbital-based anesthesia.<sup>25</sup>

**Magnetic resonance imaging.** Imaging was performed 2, 7, and 21 days after TBI or sham surgery (Table 1). All images were acquired with a two-dimensional echo sequence, as described in Appendix S1, resulting in an in-plane resolution of  $0.15 \times 0.15$  mm<sup>2</sup> with a 0.5-mm slice thickness. Note that although the sequence we used makes T2\* relaxometry possible, we used a T2\*-weighted sum-over-echoes image instead of a T2\* relaxation time image estimated from the echoes.

### 2.1.2 | EpiBioS4Rx cohort

The EpiBioS4Rx (<https://epibios.loni.usc.edu/>) is an international multicenter study funded by the National Institutes of Health with the goal of developing therapies to prevent posttraumatic epileptogenesis. The randomization and procedures carried out over the 7-month MRI follow-up of the EpiBioS4Rx animal cohort has been described in detail previously.<sup>26</sup> Here, we have analyzed the data from the University of Eastern Finland (UEF) subcohort consisting of 11 sham-operated controls and 32 rats with TBI induced with lateral FPI (nine TBI+ and 23 TBI-).

#### Animals

Adult male Sprague Dawley rats (Envigo Laboratories) were used. They were single-housed in a controlled environment (temperature = 21–23°C, humidity 50%–60%, lights on 7:00 a.m. to 7:00 p.m.) with free access to food

and water. Severe traumatic brain injury ( $2.87 \pm .82$  atm) was induced in the left hemisphere by lateral fluid percussion under 4% isoflurane anesthesia (Nnode-Ekane et al.<sup>25</sup>). Sham-operated experimental controls underwent the same anesthesia and surgical procedures without the induction of the impact.

**Magnetic resonance imaging.** Rats were imaged 2, 9, 30, and 150 days after TBI or sham surgery (Table 1) using a 7-T Bruker PharmaScan MRI scanner, as described in Appendix S1, with a resolution of  $0.16 \times 0.16 \times 0.16 \text{ mm}^3$ .

## 2.2 | Hippocampal parameters

In the following sections, we describe the process for extracting the anatomical parameters describing the left (ipsilateral to TBI) and right (contralateral) hippocampus in each scan. The EPITARGET and EpiBioS4Rx cohorts were analyzed separately.

After automatically segmenting the hippocampi and the brain mask, we defined a system of reference  $F$

specific for each brain, as detailed in Appendix S1. Then, we defined an "interpolating plane"  $P^1$  and an "inclination plane"  $P^2$  for each hippocampus (Figure 1).  $P^1$  was defined as the plane minimizing the sum of distances from hippocampus voxels to it and  $P^2$  as a plane characterizing the inclination of the hippocampus. Finally, from this geometric construction, we extracted 39 parameters describing both hippocampi and their relative positions. The parameters are listed in Table 2. The full three-dimensional (3D) construction is detailed in Appendix S1, and the 3D reconstruction in Blender 2.93<sup>27</sup> is provided in our code release.

## 2.3 | Segmentation

We segmented the brain mask and both the ipsilateral and contralateral hippocampus using MU-Net-R, which is a CNN designed for the segmentation of rat brain MRI.<sup>22,28</sup> MU-Net-R displayed segmentation performance of the hippocampus comparable with that of human raters on both datasets, with Dice overlap scores<sup>29</sup> of .92 on EpiBioS4Rx and .83 on EPITARGET.<sup>22</sup>

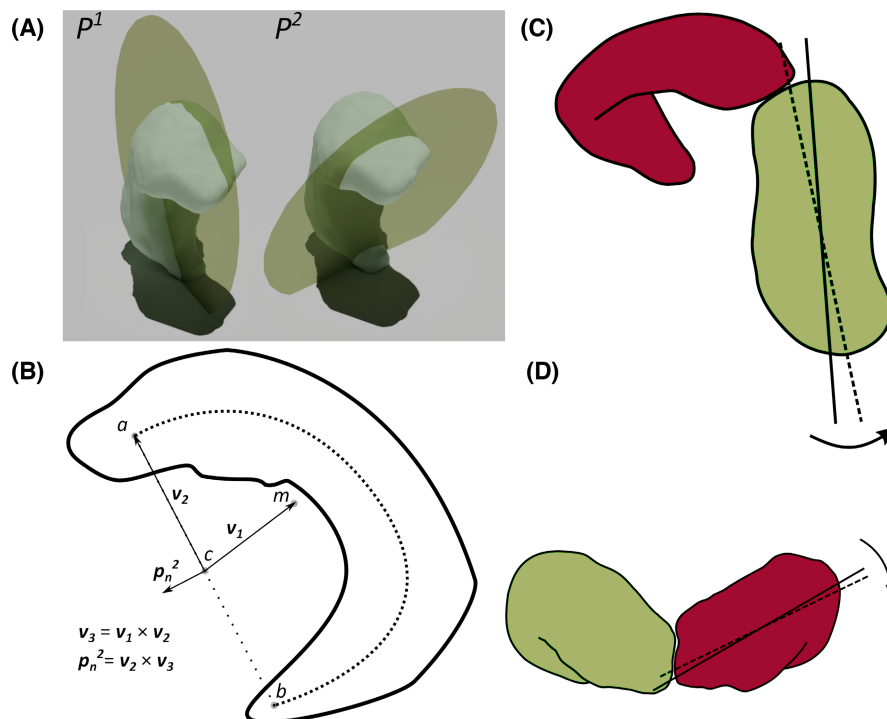


**FIGURE 1** (A) Visualization of the  $P^1$  and  $P^2$  planes in the right hippocampus of a sham-operated rat imaged at 30 days after the sham-operation (Epilepsy Bioinformatics Study for Antiepileptogenic Therapy cohort). (B) Geometric construction for the  $P^2$  plane for the segmentation mask of the hippocampus ( $H$ ).  $a$  and  $b$  indicate the extremes of the skeleton of  $H$  and  $m$  its center of mass.  $P^2$  was defined by the point  $p_p^2 = c$  and the vector  $p_n^2$ . (C, D) Average  $P^1$  shifts for the hippocampus contralateral (C) and ipsilateral (D) to the lesion. Solid lines indicate average position of  $P^1$  in non-epileptogenic animals, consistent with sketches of the hippocampi. Dashed lines indicate average position of  $P^1$  in epileptogenic animals. This shift should not be understood as a rigid translation, but as the result of an overall deformation of the hippocampus.  $v_3$  is a vector centered in  $C$  and orthogonal to the plane of the figure itself, protruding toward the reader

**TABLE 2** Parameters extracted from each scan

Parameter	Symbol
Hemispheric parameters	
Relative volumes	$v(v_{\text{ipsi}}, v_{\text{contra}})$
$P^1$ position components	$p_{\text{px}}^1, p_{\text{py}}^1, p_{\text{pz}}^1$
$P^2$ position components	$p_{\text{px}}^2, p_{\text{py}}^2, p_{\text{pz}}^2$
$P^1$ normal components	$p_{\text{nx}}^1, p_{\text{ny}}^1, p_{\text{nz}}^1$
$P^2$ normal components	$p_{\text{nx}}^2, p_{\text{ny}}^2, p_{\text{nz}}^2$
$P^1$ distance from reference	$ p_p^1 $
$P^2$ distance from reference	$ p_p^2 $
$P^1$ dihedral angle with $R$	$\theta_{1,R}$
$P^2$ dihedral angle with $R$	$\theta_{2,R}$
$P^2$ dihedral angle with $P^1$	$\theta_{1,2}$
Hemisphere independent	
Angle between $P^1$ planes	$\theta_{1,1}$
Angle between $P^2$ planes	$\theta_{1,2}$
Interhippocampal volume ratio	$v_r$

Note: The hemispheric parameters were defined for each hippocampus separately and refer to the ipsilateral (left) and contralateral hippocampus, respectively. Hemisphere independent parameters were defined for each scan, combining information from the two hippocampi.

## 2.4 | Position and orientation

### 2.4.1 | Interpolating plane $P^1$

We defined the plane  $P^1$  as an interpolating plane, minimizing the sum of distances of each voxel in the hippocampus segmentation mask  $H$  from the plane. We fitted the best interpolating plane using singular value decomposition, implemented with scikit-spatial (<https://scikit-spatial.readthedocs.io/>), and described the plane through the point  $p_p^1$  and the normal vector  $p_n^1$ .  $p_p^1$  corresponds to the center of mass of the segmentation mask, and  $p_n^1$  is selected for both hippocampi so that  $p_{\text{ny}}^1 < 0$ .

### 2.4.2 | Inclination plane $P^2$

We defined  $P^2$  to capture information about the positioning of the hippocampus complementary to that of  $P^1$ . We constructed  $P^2$  according to the following procedure, in reference to Figure 1, beginning with the extraction of the hippocampus segmentation mask  $H$ .<sup>30</sup> We identified two points at the upper and lower extremes of the skeleton,  $a$  and  $b$ . These were extracted by identifying the most rostral points in the upper and lower halves of the skeleton. Next, we identified  $c$  as the midpoint between  $a$  and  $b$ :  $c = (a + b)/2$ . The plane  $P^2$  is characterized by the point  $p_p^2 = c$  and a unit vector  $p_n^2$  orthogonal to the segment  $ab$

and lying on the plane including  $a$ ,  $b$ , and  $m$ , defined as the center of mass of  $H$ . To find  $p_n^2$  we first defined  $v_1$  as the vector pointing from  $c$  to  $m$ :  $v_1 = m - c$ . We further defined  $v_2$  as the vector pointing from  $c$  to  $a$ :  $v_2 = a - c$ . Then,  $v_3$  is expressed as the vector product  $v_3 = v_1 \times v_2$ . Finally, we defined  $p_n^2 = v_3 / |v_3|$ .

This construction is equivalent to defining  $P^2$  as the plane containing points  $a$  and  $b$  that has a maximal sum of distances from voxels in  $H$  and is characterized by a ventrally oriented normal vector.

## 2.5 | Parameters

As small inconsistencies in the positioning of each rat during each scan would constitute a source of noise, we expressed all vector components in a newly defined reference frame  $F$ .  $F$  is spanned by the unit vector  $\hat{y}$  directed in the rostral direction,  $\hat{z}$  in the dorsal direction, and  $\hat{x} = \hat{y} \times \hat{z}$ . Furthermore, the reference frame is constructed so that the plane  $R$  defined by the linear combinations of vectors  $\hat{x}$  and  $\hat{y}$  maximizes its intersection with the brain mask. For a detailed description of  $F$ , see Appendix S1.

For each scan, we extracted the following parameters. From both hippocampi, we included the volume of each hippocampus relative to the brain mask  $v_{\text{ipsi}}$  and  $v_{\text{contra}}$ , the components of vectors  $p_n^1$ ,  $p_n^2$ ,  $p_p^1$ ,  $p_p^2$ , and the dihedral angles of  $P^1$  and  $P^2$  with  $R$ , defined as  $\theta_{1,R}$  and  $\theta_{2,R}$ . We further include the dihedral angle between the ipsilateral and contralateral  $P^2$  planes  $\theta_{1,1}$ , the angle between the ipsilateral and contralateral  $P^2$  planes  $\theta_{2,2}$ , and the dihedral angles between  $P^1$  and  $P^2$  for each hippocampus, denoted as  $\theta_{1,2}$ . Lastly, we included the volume ratio between the ipsilateral and the contralateral hippocampi  $v_r = v_{\text{ipsi}}/v_{\text{contra}}$ , and the vector norms  $|p_p^1|$  and  $|p_p^2|$ , indicating the distances between the points characterizing each plane and the origin.

Because of the differences in voxel size between EpiBioS4Rx and EPITARGET, and the different anesthesia protocols, the parameters described here might not be comparable across datasets. Hence, the two were not combined during the following analyses, and were analyzed separately.

## 2.6 | Mass univariate analysis

We studied the dependency of each parameter on the timepoint and on either the presence of TBI, or according to the TBI+ and TBI− categories. We performed this by applying a repeated measures two-way analysis of variance (ANOVA), implemented in Python using the pingouin library,<sup>31</sup> with timepoint and lesion as

within-subject factors. The main effect  $p$ -values were corrected using Greenhouse–Geisser correction,<sup>32</sup> and all  $p$ -values were further corrected for multiple comparisons using Bonferroni correction.

## 2.7 | Classification

We classified the scans in two binary tasks: TBI versus sham, and TBI+ versus TBI–. We trained random forest classifiers,<sup>33</sup> implemented using scikit-learn.<sup>34</sup> To prevent overfitting, we only used trees with a depth of one (i.e., stumps), applied balanced weights to compensate for the class imbalance, and did not use bootstrapping. We trained forests of 1000 trees per classifier and optimized for the Gini impurity. We did not run any hyperparameter optimization to prevent overfitting for our small training set.

We assessed the importance of each parameter using permutation importance.<sup>33</sup> This is calculated by permuting the values for one parameter across the test data and comparing the results with the unaltered test performance. The permutation importance is then defined as the difference between the two metrics.

## 2.8 | Validation

We validated the predictions using a repeated stratified 10-fold cross-validation (CV) strategy and tested the hypothesis that the trained classifier performed better than chance using a label permutation test.<sup>35</sup> Both procedures are detailed in Appendix S1.

# 3 | RESULTS

## 3.1 | Epilepsy phenotype

### 3.1.1 | EPITARGET cohort

The prevalence of epilepsy was 29% (29 TBI+, 114 TBI–). The mean seizure frequency was  $.21 \pm .19$  seizures/day. The average seizure duration was  $89 \pm 33$  s.

### 3.1.2 | EpiBioS4Rx-UEF MRI cohort

The prevalence of epilepsy was 28% (nine TBI+, 23 TBI–). The mean seizure frequency was  $.34 \pm .64$  seizures/day. The average seizure duration was  $106 \pm 92$  s. There was no difference between the EPITARGET and EpiBioS4Rx cohorts ( $p > .05$ , Mann–Whitney).

## 3.2 | Hippocampal position and orientation

### 3.2.1 | TBI versus Sham

#### Mass univariate analysis

The repeated measures ANOVA displayed a widespread significant dependence on the timepoint across several parameters. In EPITARGET, a total of 14 parameters were significantly sensitive to the timepoint variable ( $p < .05$ ), whereas in EpiBioS4Rx, there were 25 parameters significantly sensitive to the timepoint variable. Fewer parameters were also significantly sensitive to TBI ( $p < .05$ ). In EPITARGET, these were  $v_{\text{ipsi}}$ ,  $v_r$ , the ipsilateral  $p_{\text{pz}}^2$  and  $|p_p^1|$ , and the contralateral  $|p_2|$ . In EpiBioS4Rx, these were the ipsilateral  $p_{\text{py}}^1$ ,  $p_{\text{py}}^2$ , and  $|p_p^1|$ . All these parameters were sensitive to TBI also in combination with timepoint, as a second order effect. No parameter was significantly affected by TBI independently of the timepoint. For a full breakdown of effect sizes and  $p$ -values, see Appendix S1.

#### Classification

We trained random forests to classify TBI versus sham rats separately for each timepoint. Table 3 reports the mean and SD across the folds of the stratified 10-fold CV procedure. The random forest was highly effective in discriminating between these two classes for all timepoints, achieving balanced accuracy of 90% or higher. The only exception was the 9-day timepoint in the EpiBioS4Rx dataset, with a balanced accuracy of .627. As a general trend, the classification quality metrics were higher in the EPITARGET than EpiBioS4Rx dataset, with larger scores when averaged across all timepoints. This result still held true when ignoring the 9-day timepoint. For both datasets, we observed a higher average sensitivity (EPITARGET, .9724; EpiBioS4Rx, .9062) and positive predictive value (.9823, .9317) than specificity (.9145, .8091) and negative predictive value (.8784, .7517). Likewise, we measured higher average precision (.9823, .9317) and lower recall (.9725, .9062), with average F1 scores of .9773 and .9185. Receiver operating characteristic curves generated for both datasets are displayed in Figure 2, with all classifiers achieving a high AUC ( $>.96$ ) except for the 9-day timepoint in EpiBioS4Rx.

We report the parameter importance plot for the 2-day and the 150-day timepoints in Figure 3. The parameter importance plots for all timepoints are provided in Appendix S1. In the EPITARGET dataset, the most important parameter for the 2-day timepoint was the ipsilateral  $|p_p^1|$ , followed by smaller contributions from  $p_{\text{py}}^1$ , the contralateral  $|p_2|$ ,  $\theta_{1,1}$ , and  $\theta_{2,2}$ . Volumetric parameters only had a minor contribution to classifiers at 2 days. In the EpiBioS4Rx dataset, the most important parameters were

**TABLE 3** Random forest performance for each imaging timepoint in sham versus TBI and TBI+ versus TBI- (nonepileptic) classification in EpiBioS4Rx and EPITARGET cohorts

MRI, days	Acc	p	BAcc	p	Sen	p	Spec	p	PPV	p	NPV	p	Prec	p	Recall	p	F1	p	
EpiBioS4Rx cohort sham versus TBI																			
2	.977	.0001	.9844	.0001	.969	.0008	1	.0001	1	.0001	.917	.0001	1	.0001	.9688	.0008	.984	.0001	
9	.705	.1655	.627	.1086	.794	.1722	.455	.1999	.803	.2726	.449	.1109	.8034	.2726	.7935	.1722	.798	.1917	
9*	.767	.0434	.7246	.0261	.813	.0701	.636	.0675	.863	.0989	.553	.0301	.8627	.0989	.8129	.0701	.837	.059	
30	.94	.0001	.9339	.0001	.941	.004	.936	.0001	.978	.0001	.846	.0002	.9776	.0001	.9406	.004	.959	.0004	
150	.902	.0003	.8943	.0001	.922	.0035	.846	.001	.946	.0014	.795	.0002	.9458	.0012	.9219	.0035	.933	.0009	
EPITARGET cohort sham versus TBI																			
2	.956	.0001	.9132	.0001	.978	.0001	.852	.0006	.97	.0002	.887	.0001	.97	.0002	.9777	.0001	.974	.0001	
7	.94	.0001	.919	.0001	.947	.0001	.909	.0001	.98	.0001	.782	.0001	.9804	.0001	.9468	.0001	.963	.0001	
21	.991	.0001	.9891	.0001	.993	.0001	.983	.0001	.997	.0001	.966	.0001	.9965	.0001	.9929	.0001	.995	.0001	
EpiBioS4Rx cohort TBI+ versus TBI-																			
2	.528	.7441	.3961	.7988	.156	.7607	.674	.6054	.161	.732	.67	.7408	.1613	.732	.1556	.7607	.157	.752	
9	.568	.5933	.4704	.5552	.25	.54	.678	.5781	.22	.5708	.721	.5327	.2196	.5708	.25	.54	.232	.5633	
30	.584	.6138	.4804	.5315	.322	.4904	.687	.6015	.295	.5157	.72	.5993	.2948	.5157	.3222	.4904	.305	.5168	
150	.809	.0296	.7998	.0054	.767	.0089	.826	.1236	.636	.0223	.9	.0247	.6361	.0223	.7667	.0089	.694	.0078	
EPITARGET cohort TBI+ versus TBI-																			
2	.554	.519	.5279	.3262	.497	.2428	.574	.6637	.289	.3805	.765	.3922	.2894	.3805	.4966	.2428	.365	.3166	
7	.598	.2338	.5913	.0839	.597	.0922	.599	.4639	.345	.1718	.808	.1645	.3447	.1718	.5966	.0922	.437	.1144	
21	.587	.2902	.5142	.4122	.359	.605	.666	.2093	.271	.4293	.75	.4475	.2711	.4293	.3586	.605	.308	.5081	

Note: "9\*" refers to the classifier we trained on the 9-day EpiBioS4Rx dataset, using the top 10 parameters in order of importance from the 7-day EPITARGET dataset.

Abbreviations: Acc, accuracy; BAcc, balanced accuracy; EpiBioS4Rx, Epilepsy Bioinformatics Study for Antiepileptogenic Therapy; MRI, magnetic resonance imaging; NPV, negative predictive value; PPV, positive predictive value; Prec, precision; Sen, sensitivity; Spec, specificity; TBI, traumatic brain injury.

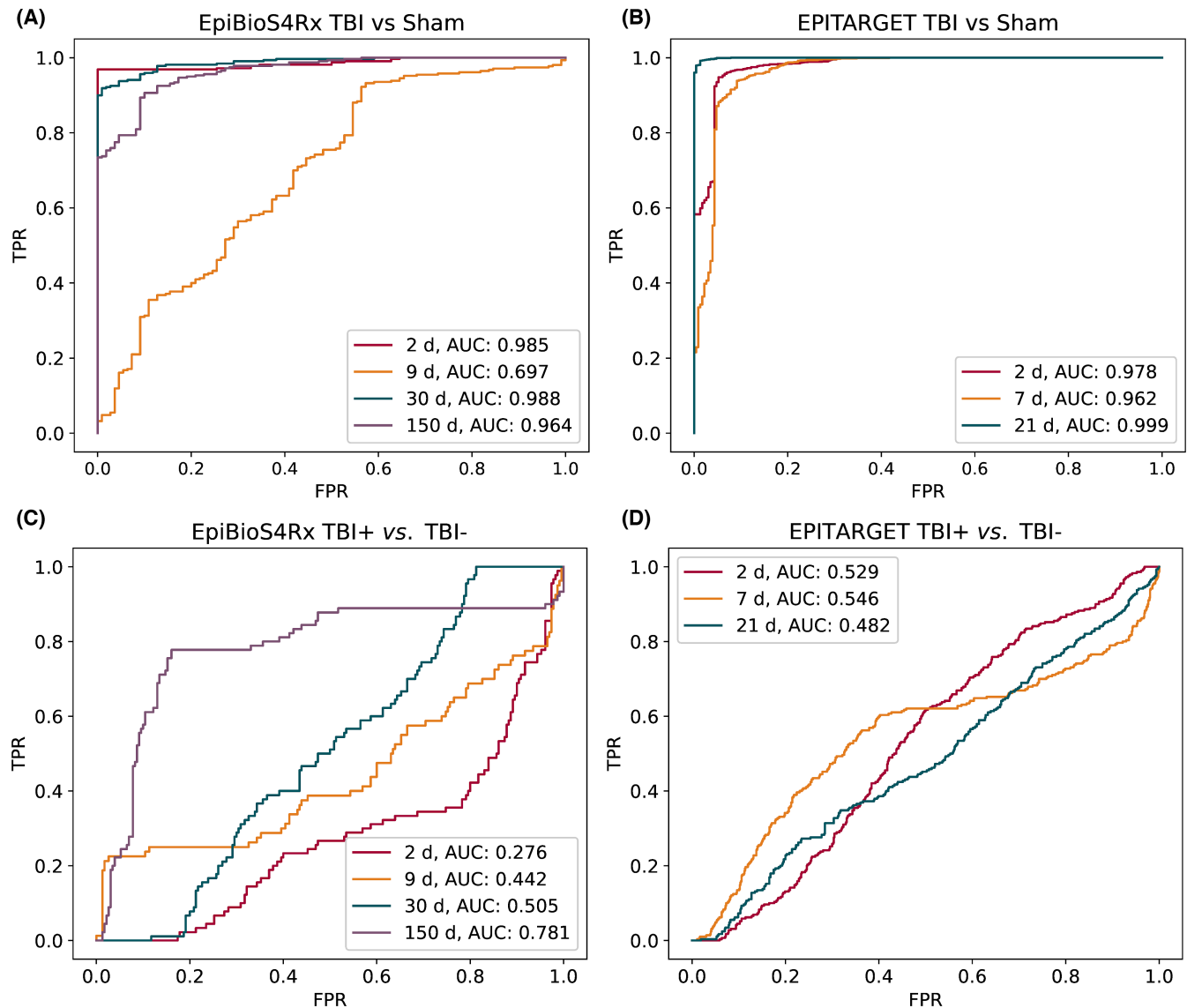


**FIGURE 2** (A, B) Receiver operating characteristic (ROC) curves for all timepoints in traumatic brain injury (TBI) versus sham classification in the Epilepsy Bioinformatics Study for Antiepileptogenic Therapy (EpiBioS4Rx) (left) and EPITARGET (right) animal cohorts. The random forest-estimated probability of TBI, based on the hippocampal parameters, reached a high area under the curve (AUC) at each timepoint except the 9-day EpiBioS4Rx timepoint. (C, D) ROC curves for rats with epilepsy (TBI+) versus no epilepsy (TBI-) classifiers, across all timepoints in the EpiBioS4Rx and EPITARGET datasets. At earlier timepoints, the classifiers did not discriminate between the TBI+ and TBI- animals. However, in the EpiBioS4Rx cohort imaged at the 150-day timepoint, the hippocampal parameters effectively discriminated between the TBI+ and TBI- animals. FPR, false positive rate; TPR, true positive rate

the ipsilateral  $\theta_{1,R}$ ,  $p_{nz}^1$  (indicating the  $z$  component of  $p_n^1$ ), and  $p_{px}^1$ , with a minor contribution from  $v_r$ .

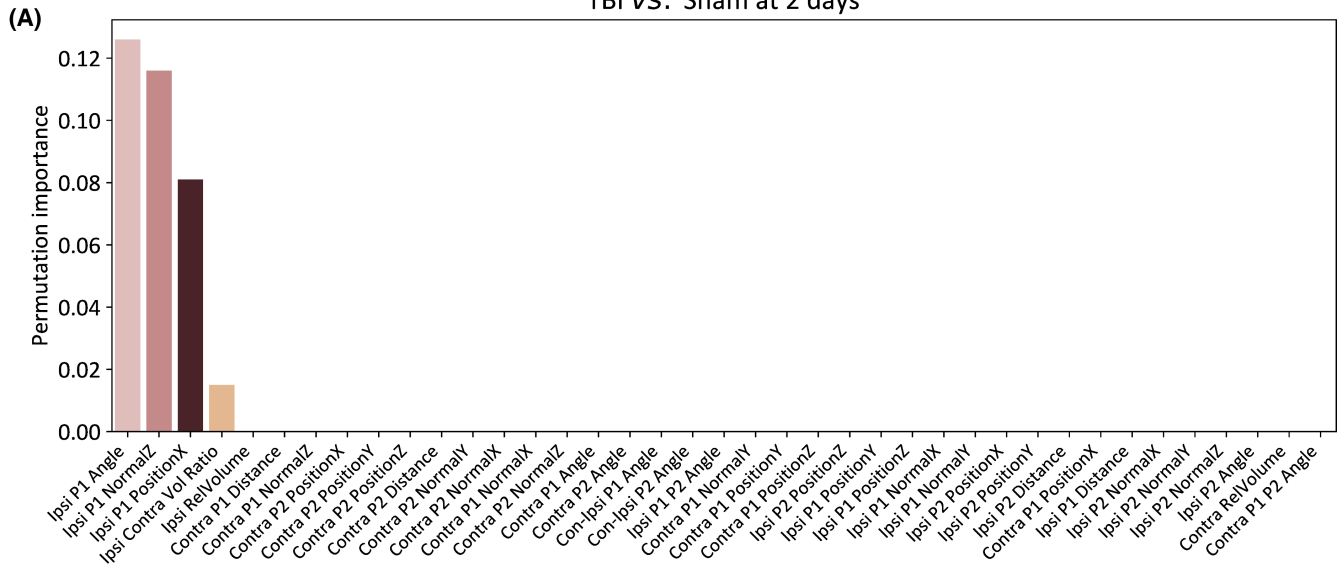
In contrast, for the later timepoints of 7, 21, 30, and 150 days, the most important parameters were  $v_r$  followed by  $v_{ipsi}$ . With respect to the 9-day timepoint in the

EpiBioS4Rx dataset, where the classifier did not perform well, we found ipsilateral  $\theta_{1,R}$ , the contralateral  $v_{contra}$  and  $p_{px}^1$ , and the ipsilateral  $p_{py}^1$  to be the most relevant parameters. These were different than the important parameters in the other timepoints of  $\geq 7$  days. However, by retraining

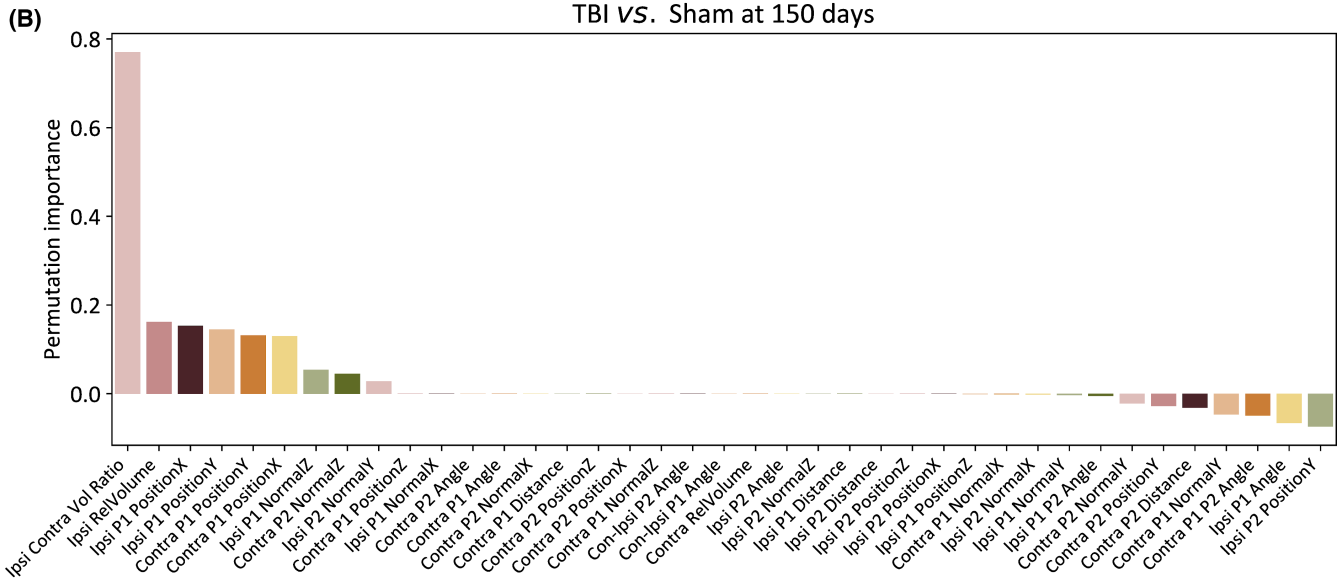
**FIGURE 3** Parameter importance for the (A) 2-day and (B) 150-day timepoint classification of sham versus traumatic brain injury (TBI) animals in the Epilepsy Bioinformatics Study for Antiepileptogenic Therapy dataset. Whereas for the 2-day timepoint, the most important parameters describe the orientation and positioning of the hippocampus through the plane, for later timepoints, the hippocampal volume was the most important factor. (C) The 150-day timepoint classification of the epilepsy (TBI+) versus no epilepsy (TBI-) animals. The most important parameters discriminating the two groups were the  $P^1$  parameters of the ipsilateral and contralateral hippocampi. Contra or Con, contralateral hippocampus; Ipsi, ipsilateral hippocampus; Pi NormalK,  $p_{nk}^1$ ; Pi PositionK,  $p_{pk}^1$ ; Vol, volume; RelVol, relative volume



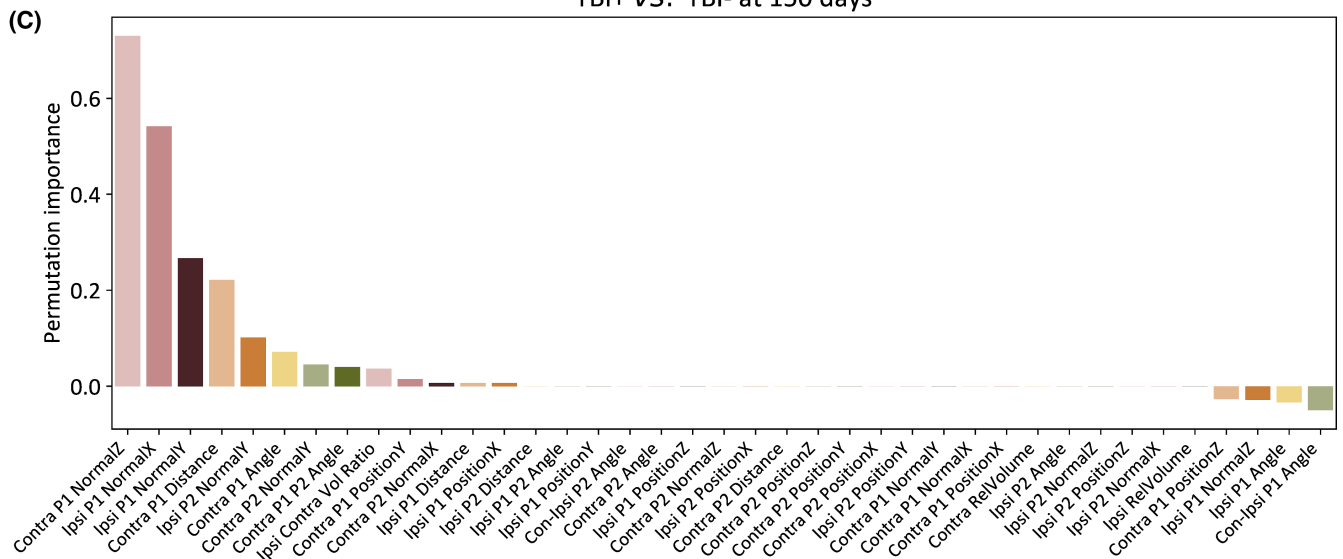
TBI vs. Sham at 2 days



TBI vs. Sham at 150 days



TBI+ vs. TBI- at 150 days



this classifier only selecting the top 10 parameters by importance on the 7-day EPITARGET classifier, we obtained improved performance (balanced accuracy = .7246,  $p = .0261$ ), indicated as 9\* in Table 3.

### 3.2.2 | TBI+ versus TBI–

#### Mass univariate analysis

As described in the TBI versus sham analysis, many of the parameters were dependent on the timepoint variable, and unsurprisingly, this was verified in the TBI+ versus TBI– analysis also. However, no parameter displayed a significant dependence on TBI+ in the multivariate ANOVA analysis, neither when considered individually nor in combination with the timepoint, across both datasets. For a full breakdown of effect sizes and  $p$ -values, we refer the reader to Appendix S1.

#### Classification

Next, we trained a random forest to discriminate between TBI+ and TBI– rats. In the EpiBioS4Rx dataset, the 150-day timepoint revealed a high balanced accuracy of .7998 ( $p = .0054$ ) and an F1 score of .6944 ( $p = .00779$ ), as reported in more detail in Table 3. For all other timepoints for both datasets, we did not obtain classifiers that would have been significantly better than the chance level (50% balanced accuracy).

According to permutation importance, the two most important parameters in the 150-day EpiBioS4Rx dataset discriminating the TBI+ and TBI– animals were the contralateral  $p_{nz}^1$  and the ipsilateral  $p_{nx}^1$ . These were followed by the ipsilateral  $p_{ny}^1$ , the contralateral  $|p_n^1|$ , and parameters of lower importance as displayed in Figure 3. Parameter importance for all other timepoints is reported in Appendix S1.

## 4 | DISCUSSION

Over the course of weeks to months, TBI induces substantial atrophy of the brain, accompanied by a ventricle enlargement and changes in the position and orientation of periventricular structures such as the hippocampus. Here, our objective was to identify prognostic biomarkers for PTE using parameters derived from the repositioning of the atrophied hippocampus during the post-TBI aftermath. We automatically segmented two large  $T_2^*$  MRI datasets and extracted a set of parameters describing the position and orientation of the ipsilateral and contralateral hippocampus over the course of 5 post-TBI months, which overlaps with the evolution of PTE. Our data show that these parameters can differentiate the sham-operated

and TBI animals with high sensitivity and specificity. At the more advanced stages of post-TBI structural alterations (i.e., 5 months post-TBI), the changed position and orientation of the hippocampus also differentiate the epileptic from nonepileptic animals.

### 4.1 | Hippocampal parameters differentiating TBI animals from sham-operated experimental controls show time-dependency

Previous histologic studies have shown progressive pathology in the principal cells and interneurons of the dentate gyrus and hippocampus proper after lateral FPI-induced TBI.<sup>36</sup> Moreover, our previous 11-month MRI follow-up of animals after lateral FPI revealed progressive diffusion changes in the ipsilateral hippocampus for up to 3 months postinjury, which were substantially milder contralaterally.<sup>37</sup> Here, we report that the hippocampal position and orientation were highly effective in differentiating TBI rats from the sham-operated animals, starting at 2 days postinjury for up to 5 months. Interestingly, the parameters contributing to the classification at different imaging timepoints varied. At the early 2-day post-TBI timepoint, the most important parameters described the orientation of  $P^1$ , that is, the plane cutting the ipsilateral hippocampus into two halves along its septotemporal axis, indicating rotation. At 7, 21, 30, and 150 days, the reduction in ipsilateral/contralateral volume ratio ( $v_r$ ) showed the best predictive value. The poor performance of the classifier at the 9-day timepoint could be attributed to overfitting. This was evident as the performance markedly increased, when we limited the classification to the top 10 parameters by importance as calculated on the 7-day timepoint in the EPITARGET dataset, which was the closest timepoint to 9-day imaging in the EpiBioS4Rx cohort.

### 4.2 | Hippocampal parameters measured at 5 months post-TBI performed best in differentiating epileptic and nonepileptogenic animals

Next, we assessed whether the geometric parameters captured early postinjury could differentiate between the animals that would later develop epilepsy and those that would not. Unfortunately, no single variable was significantly effective in discriminating between TBI+ and TBI– animals after Bonferroni correction, suggesting that a linear univariate model is not sufficiently complex to discriminate between the two categories. However, by combining multiple parameters and using random forest

classifiers, we could effectively discriminate the epileptogenic from the nonepileptogenic animals at the 150-day timepoint. The important parameters for discrimination were primarily the geometric parameters describing both  $P^1$  planes, indicating the rotation of both hippocampi along their longitudinal septotemporal axis. Unlike in sham versus TBI classification, early volume reduction played a minor role. The parameter importance evaluation indicated that the ipsilateral hippocampus had rotated counterclockwise toward the lateral direction. Somewhat unexpectedly, the most important feature differentiating the TBI+ and TBI− animals was present in the contralateral hippocampus, its  $P^1$  plane turning away from the vertical direction.

Our present findings agree with previous studies showing that hippocampal changes assessed at 6–9 months after TBI differentiate between epileptogenic and nonepileptogenic animals, even though no statistics for differentiation accuracy were provided by earlier reports.<sup>10,19,20</sup> Interestingly, in the EPITARGET cohort analyzed here, we recently showed that thalamic diffusion changes differentiated epileptogenic from nonepileptogenic animals already during the first postinjury weeks.<sup>38</sup> Instead, the severity of cortical damage or its progression were without prognostic value.<sup>26</sup> These data suggest that whole-brain multimodal MRI analysis could prove highly valuable in the study of epileptogenesis and its biomarkers.

### 4.3 | Limitations

Although the EPITARGET dataset was large, including 170 animals imaged at three timepoints, MRI was performed at a low resolution. The lower resolution could have concealed information that would have emerged from a dataset of the same size, containing images with a smaller voxel size. Second, the last imaging dataset analyzed in the EPITARGET cohort was at 21 days post-TBI. Thus, we could not replicate the promising findings observed in the 150-day dataset of the EpiBioS4Rx cohort in the EPITARGET cohort. These shortcomings likely explain the fewer parameters detected as significantly dependent on the timepoint in the repeated measures ANOVA in the EPITARGET cohort. Conversely, EpiBioS4Rx suffers from the smaller dataset size, including only 43 animals, which is likely one of the factors causing the overfitting problem. If the high-resolution EpiBioS4Rx dataset had been even larger, we might have been able to identify a prognostic biomarker for PTE even earlier than the 5-month chronic timepoint. The above differences in the two datasets prevented us from combining them in the analysis, and therefore, they were analyzed separately.

## 5 | CONCLUSIONS

TBI-induced chronic hippocampal deformation detected by clinically translatable MRI methodologies identified subjects at high risk of PTE after experimental TBI. As the orientation of hippocampus in the temporal lobe and its exposure to TBI-related mechanical forces in humans differs from that in the rat lateral FPI model, the specific parameters derived from the animal study are unlikely to preserve the same meaning when applied to the human brain. However, the general approach can be extended to human TBI and epilepsy syndromes with abnormal hippocampal shape and orientation.<sup>10,39</sup> Our study provides a testable hypothesis that parameters reporting on the position and orientation of the hippocampus bilaterally could reflect the severity of brain pathology and serve as prognostic biomarkers for posttraumatic epileptogenesis beyond rodent models, paving the way toward subject stratification for antiepileptogenesis studies.

### ACKNOWLEDGMENTS

We thank Jarmo Hartikainen, Merja Lukkari, and Michele Allori for their excellent technical assistance. This study was supported by the Medical Research Council and Natural Science and Engineering Research Council of the Academy of Finland (272249, 273909, 2285733-9, 298007, 316258), the Sigrid Juselius Foundation, the European Union's Seventh Framework Program (FP7/2007-2013) under grant agreement 602102 (EPITARGET), the National Institute of Neurological Disorders and Stroke Center Without Walls of the National Institutes of Health under award number U54NS100064 (EpiBioS4Rx), grant S21770 from the European Social Fund, and grant 65211916 from the North Savo Regional Fund (R.D.F.).

### CONFLICT OF INTEREST

None of the authors has any conflict of interest to disclose. We confirm that we have read the Journal's position on issues involved in ethical publication and affirm that this report is consistent with those guidelines.

### DATA AVAILABILITY STATEMENT

The code used in our work and an example 3D model of our geometric construction are freely available under the MIT license at <https://github.com/Hierakonpolis/RatHippocampusGeometry>. The MRI data are stored on University of Eastern Finland servers and will be made available upon request.

### ORCID

Riccardo De Feo  <https://orcid.org/0000-0001-7510-1058>  
 Eppu Manninen  <https://orcid.org/0000-0002-9353-6079>  
 Asla Pitkänen  <https://orcid.org/0000-0002-8163-5416>  
 Jussi Tohka  <https://orcid.org/0000-0002-1048-5860>

## REFERENCES

- World Health Organization. Epilepsy: A Public Health Imperative. Geneva, Switzerland: World Health Organization; 2019.
- Scheffer IE, Berkovic S, Capovilla G, Connolly MB, French J, Guilhoto L, et al. ILAE classification of the epilepsies: position paper of the ILAE Commission for Classification and Terminology. *Epilepsia*. 2017;58(4):512–21.
- Dulla CG, Pitkänen A. Novel approaches to prevent epileptogenesis after traumatic brain injury. *Neurotherapeutics*. 2021;18(3):1582–601. <https://doi.org/10.1007/s13311-021-01119-1>
- Engel J, Pitkänen A, Loeb JA, Dudek FE, Bertram EH, Cole AJ, et al. Epilepsy biomarkers. *Epilepsia*. 2013;54:61–9. <https://doi.org/10.1111/epi.12299>
- Annegers JF, Hauser WA, Coan SP, Rocca WA. A population-based study of seizures after traumatic brain injuries. *N Engl J Med*. 1998;338(1):20–4.
- Christensen J. Traumatic brain injury: risks of epilepsy and implications for medicolegal assessment. *Epilepsia*. 2012;53:43–7.
- Haltiner AM, Temkin NR, Dikmen SS. Risk of seizure recurrence after the first late posttraumatic seizure. *Arch Phys Med Rehabil*. 1997;78(8):835–40. [https://doi.org/10.1016/S0003-9993\(97\)90196-9](https://doi.org/10.1016/S0003-9993(97)90196-9)
- Gupta PK, Sayed N, Ding K, Agostini MA, Van Ness PC, Yablon S, et al. Subtypes of post-traumatic epilepsy: clinical, electrophysiological, and imaging features. *J Neurotrauma*. 2014;31(16):1439–43.
- Kharatishvili I, Nissinen JP, McIntosh TK, Pitkänen A. A model of posttraumatic epilepsy induced by lateral fluid-percussion brain injury in rats. *Neuroscience*. 2006;140(2):685–97.
- Shultz SR, Cardamone L, Liu YR, Hogan RE, Maccotta L, Wright DK, et al. Can structural or functional changes following traumatic brain injury in the rat predict epileptic outcome? *Epilepsia*. 2013;54(7):1240–50.
- Churn S, Campbell JN, Gandhi A, Singh B. Traumatic brain injury causes a tacrolimus-sensitive increase in non-convulsive seizures in a rat model of post-traumatic epilepsy. *Int J Neurol Brain Disord*. 2014;1(1):1–11. <https://doi.org/10.15436/2377-1348.14.002>
- Reid AY, Bragin A, Giza CC, Staba RJ, Engel J. The progression of electrophysiologic abnormalities during epileptogenesis after experimental traumatic brain injury. *Epilepsia*. 2016;57(10):1558–67.
- Wang X, Wang Y, Zhang C, Liu C, Yang H-F, Wen-Han HU, et al. Endogenous cannabinoid system alterations and their role in epileptogenesis after brain injury in rat. *Epilepsy Res*. 2016;128:35–42.
- Nissinen J, Andrade P, Natunen T, Hiltunen M, Malm T, Kanninen K, et al. Disease-modifying effect of atipamezole in a model of post-traumatic epilepsy. *Epilepsy Res*. 2017;136:18–34. <https://doi.org/10.1016/j.epilepsyres.2017.07.005>
- Bragin A, Li L, Almajano J, Alvarado-Rojas C, Reid AY, Staba RJ, et al. Pathologic electrographic changes after experimental traumatic brain injury. *Epilepsia*. 2016;57(5):735–45. <https://doi.org/10.1111/epi.13359>
- Huttunen JK, Airaksinen AM, Barba C, Colicchio G, Niskanen J-P, Shatillo A, et al. Detection of hyperexcitability by functional magnetic resonance imaging after experimental traumatic brain injury. *J Neurotrauma*. 2018;35(22):2708–17. <https://doi.org/10.1089/neu.2017.5308>
- Swartz BE, Houser CR, Tomiyasu U, Walsh GO, DeSalles A, Rich JR, et al. Hippocampal cell loss in posttraumatic human epilepsy. *Epilepsia*. 2006;47(8):1373–82.
- Santhakumar V, Bender R, Frotscher M, Ross ST, Hollrigel GS, Toth Z, et al. Granule cell hyperexcitability in the early post-traumatic rat dentate gyrus: the ‘irritable mossy cell’ hypothesis. *J Physiol*. 2000;524(1):117–34.
- Kharatishvili I, Immonen R, Gröhn O, Pitkänen A. Quantitative diffusion MRI of hippocampus as a surrogate marker for post-traumatic epileptogenesis. *Brain*. 2007;130(12):3155–68.
- Hayward NMEA, Immonen R, Tuunanen PI, Nnode-Ekane XE, Gröhn O, Pitkänen A. Association of chronic vascular changes with functional outcome after traumatic brain injury in rats. *J Neurotrauma*. 2010;27(12):2203–19.
- Pitkänen A, Immonen R. Epilepsy related to traumatic brain injury. *Neurotherapeutics*. 2014;11(2):286–96.
- De Feo R, Hämäläinen E, Manninen E, Immonen R, Valverde JM, Nnode-Ekane XE, et al. Convolutional neural networks enable robust automatic segmentation of the rat hippocampus in MRI after traumatic brain injury. *Front Neurol*. 2022;13:1664–2295. <https://doi.org/10.3389/fneur.2022.820267>
- O’Shea K, Nash R. An introduction to convolutional neural networks. arXiv preprint. arXiv: 1511.08458, 2015.
- Abbasi B, Goldenholz DM. Machine learning applications in epilepsy. *Epilepsia*. 2019;60(10):2037–47.
- Nnode-Ekane XE, Santana-Gomez C, Casillas-Espinosa PM, Ali I, Brady RD, Smith G, et al. Harmonization of lateral fluid-percussion injury model production and post-injury monitoring in a preclinical multicenter biomarker discovery study on post-traumatic epileptogenesis. *Epilepsy Res*. 2019;151:7–16.
- Manninen E, Chary K, Lapinlampi N, Andrade P, Paananen T, Sierra A, et al. Early increase in cortical t2 relaxation is a prognostic biomarker for the evolution of severe cortical damage, but not for epileptogenesis, after experimental traumatic brain injury. *J Neurotrauma*. 2020;37(23):2580–94.
- Blender Online Community. Blender—a 3D Modelling and Rendering Package. Amsterdam, the Netherlands: Blender Foundation; 2018. <http://www.blender.org>
- De Feo R, Shatillo A, Sierra A, Valverde JM, Gröhn O, Giove F, et al. Automated joint skull-stripping and segmentation with Multi-Task U-Net in large mouse brain MRI databases. *NeuroImage*. 2021;229:117734.
- Dice LR. Measures of the amount of ecologic association between species. *Ecology*. 1945;26(3):297–302.
- Zhang TY, Suen CY. A fast parallel algorithm for thinning digital patterns. *Commun ACM*. 1984;27(3):236–9.
- Vallat R. Pingouin: statistics in Python. *J Open Source Soft*. 2018;3(31):1026.
- Greenhouse SW, Geisser S. On methods in the analysis of profile data. *Psychometrika*. 1959;24(2):95–112.
- Breiman L. Random forests. *Mach Learn*. 2001;45(1):5–32.
- Pedregosa F, Varoquaux G, Gramfort A, Michel V, Thirion B, Grisel O, et al. Scikit-learn: machine learning in Python. *J Mach Learn Res*. 2011;12:2825–30.

35. Ojala M, Garriga GC. Permutation tests for studying classifier performance. *J Mach Learn Res.* 2010;11(62):1833–63.
36. Pitkänen A, McIntosh TK. Animal models of post-traumatic epilepsy. *J Neurotrauma.* 2006;23(2):241–61.
37. Immonen RJ, Kharatishvili I, Niskanen J-P, Gröhn H, Pitkänen A, Gröhn OHJ. Distinct MRI pattern in lesional and perilesional area after traumatic brain injury in rat—11 months follow-up. *Exp Neurol.* 2009;215(1):29–40.
38. Manninen E, Chary K, Lapinlampi N, Andrade P, Paananen T, Sierra A, et al. Acute thalamic damage as a prognostic biomarker for post-traumatic epileptogenesis. *Epilepsia.* 2021;62(8):1852–64.
39. Bernasconi N, Natsume J, Bernasconi A. Progression in temporal lobe epilepsy: differential atrophy in mesial temporal structures. *Neurology.* 2005;65(2):223–8.

## SUPPORTING INFORMATION

Additional supporting information may be found in the online version of the article at the publisher's website.

**How to cite this article:** De Feo R, Manninen E, Chary K, Hämäläinen E, Immonen R, Andrade P, et al. Hippocampal position and orientation as prognostic biomarkers for posttraumatic epileptogenesis: An experimental study in a rat lateral fluid percussion model. *Epilepsia.* 2022;63:1849–1861. <https://doi.org/10.1111/epi.17264>